\



Pressure dependence of the thermal stability in $LiMn_2O_4$

Yan Zeng(曾彦), Hao Liang(梁浩), Shixue Guan(管诗雪), Junpu Wang(王俊普), Wenjia Liang(梁文嘉), Mengyang Huang(黄梦阳), and Fang Peng(彭放)

Citation: Chin. Phys. B, 2022, 31 (**1**): 016104. DOI: 10.1088/1674-1056/ac1932
Journal homepage: http://cpb.iphy.ac.cn; http://iopscience.iop.org/cpb

What follows is a list of articles you may be interested in

Prediction of scandium tetraboride from first-principles calculations: Crystal structures, phase stability, mechanical properties,and hardness

Bin-Hua Chu(初斌华) and Yuan Zhao(赵元)
Chin. Phys. B, 2021, 30 (**7**): 076107. DOI: 10.1088/1674-1056/abe116

Novel rubidium polyfluorides with F_3, F_4, and F_5 species

Ziyue Lin(林子越), Hongyu Yu(于洪雨), Hao Song(宋昊), Zihan Zhang(张子涵), Tianxiao Liang(梁天笑), Mingyang Du(杜明阳), and Defang Duan(段德芳)
Chin. Phys. B, 2021, 30 (**6**): 066102. DOI: 10.1088/1674-1056/abefc6

Ground-state structure and physical properties of YB_3 predicted from first-principles calculations

Bin-Hua Chu(初斌华), Yuan Zhao(赵元), and De-Hua Wang(王德华)
Chin. Phys. B, 2021, 30 (**4**): 046101. DOI: 10.1088/1674-1056/abcf94

Ab initio study on crystal structure and phase stability of ZrC_2 under high pressure

Yong-Liang Guo(郭永亮), Jun-Hong Wei(韦俊红), Xiao Liu(刘潇), Xue-Zhi Ke(柯学志), and Zhao-Yong Jiao(焦照勇)
Chin. Phys. B, 2021, 30 (**1**): 016101. DOI: 10.1088/1674-1056/abb3e7

Synthesis, structure, and properties of $Ba_9Co_3Se_{15}$ with one-dimensional spin chains

Lei Duan(段磊), Xian-Cheng Wang(望贤成), Jun Zhang(张俊), Jian-Fa Zhao(赵建发), Li-Peng Cao(曹立朋), Wen-Min Li(李文敏), Run-Ze Yu(于润泽), Zheng Deng(邓正), Chang-Qing Jin(靳常青)
Chin. Phys. B, 2020, 29 (**3**): 036102. DOI: 10.1088/1674-1056/ab69ea

---

Pressure dependence of the thermal stability in $LiMn_2O_4$

Yan Zeng(曾彦)[1], Hao Liang(梁浩)[2,‡], Shixue Guan(管诗雪)[1], Junpu Wang(王俊普)[1], Wenjia Liang(梁文嘉)[1], Mengyang Huang(黄梦阳)[1], and Fang Peng(彭放)[1,†]

[1] *Institute of Atomic and Molecular Physics, Sichuan University, Chengdu* 610065, *China*
[2] *School of Science, Southwest University of Science and Technology, Mianyang* 621010, *China*

(Received 30 May 2021; revised manuscript received 20 July 2021; accepted manuscript online 30 July 2021)

Structural stability in terms of the decomposition temperature in $LiMn_2O_4$ was systematically investigated by a series of high-temperature and high-pressure experiments. $LiMn_2O_4$ was found to have structural stability up to 5 GPa at room temperature. Under ambient pressure, the compound decomposed at 1300 °C. The decomposition temperature decreased with increasing pressure, yielding more complex decomposed products. Below the decomposition temperature, the crystal structure of $LiMn_2O_4$ varied with pressure. The presented results in this study offer new insights into the thermal and pressure stability of $LiMn_2O_4$ materials as a cathode for lithium-ion batteries that can operate under extreme conditions. Therefore, these findings may serve as a useful guide for future work for improving lithium-ion batteries.

Keywords: $LiMn_2O_4$, high pressure, x-ray diffractometer, decomposition reactions

PACS: 61.05.cp, 82.30.Lp **DOI:** 10.1088/1674-1056/ac1932

1. Introduction

Spinel-type lithium manganese oxide ($LiMn_2O_4$, space group *Fd-3m*) is widely used as a cathode material for lithium-ion batteries. $LiMn_2O_4$ may be regarded as the most common alternative to lithium cobalt oxide ($LiCoO_2$) because Mn is abundant in nature and can reduce the cost of lithium-ion batteries.[1–5] Nowadays, $LiMn_2O_4$ cathodes are commonly found in lithium-ion batteries used in sustainable energy vehicles.[6] The investigation of different properties of $LiMn_2O_4$ under high temperature and high pressure is a promising strategy to rationalize the ideal synthesis conditions and thermal modifications of $LiMn_2O_4$. For $LiMn_2O_4$, there are many synthesis procedures available, including conventional solid-state synthesis, citric acid assisted sol–gel route synthesis and several novel techniques, such as the explosion or detonation method, which involves temperature and pressure.[7,8] The explosion process usually occurs instantly, so it is difficult to observe and develop a deeper understanding of this process. Nevertheless, by simulating the high temperature and high-pressure environment during synthesis, is possible to gain some insights into the synthesis process and the properties of the final $LiMn_2O_4$ product.

The effects of high pressure and/or high temperature (HPHT) on the phase transition of $LiMn_2O_4$ have been studied extensively in recent decades. Paolone *et al.*[9] reported that spinel $LiMn_2O_4$ will be distorted when the pressure rises above 10 GPa at room temperature, forming a metastable state, whereas Yamaura *et al.*[10] showed that $LiMn_2O_4$ undergoes a phase transition from the original spinel to the $CaFe_2O_4$ (calcium ferrite)-type structure under 6 GPa at temperatures above 1100 °C. Mukai *et al.*[11] synthesized $CaFe_2O_4$-type $LiMn_2O_4$ (CF-LMO) under high pressure (12.0 GPa) and studied its electrochemical properties and crystal structure. They reported that the $LiMn_2O_4$ spinel converts into a CF-LMO structure above 800 °C. Lin *et al.*[12] studied the related $LiMn_2O_4$ compound. They demonstrated that $LiMn_2O_4$ undergoes a reversible phase transition from a cubic structure to a tetragonal structure at 11.0 GPa (room temperature), where the bulk elastic modulus of the cubic structure was found to be 119(4) GPa. Darul *et al.*[13] showed that $LiMn_2O_4$ undergoes a structural phase transition from cubic to tetragonal due to Jahn–Teller distortion at 4.0 GPa. Heating up to about 600 K under 4.0 GPa leads to the reverse phase transition, and the tetragonal phase transforms back to the cubic one. Furthermore, they showed that HP effects decrease the temperature of decomposition, where Mn_3O_4 and MnO secondary phases appear. However, no explanation as to why this occurs was given.

To investigate the decomposition behavior of $LiMn_2O_4$, it is useful to study how HTHP affects the structural stability. This will help to rationalize the synthesis and modification of $LiMn_2O_4$ cathode materials for lithium-ion batteries. In this work, we studied the decomposition of $LiMn_2O_4$ at 2.0 GPa–5.0 GPa in a temperature range of 25 °C–1000 °C while using a cubic press (DS6 × 14 MN, China). The obtained products after HPHT experiments were then characterized by *in-situ* x-ray diffraction (XRD) and scanning electron microscopy (SEM).

†Corresponding author. E-mail: pengfang@scu.edu.cn
‡Corresponding author. E-mail: lianghao@swust.edu.cn

© 2022 Chinese Physical Society and IOP Publishing Ltd

2. Materials and experimental methods

$LiMn_2O_4$ (Fd-$3m$) powder (purity $> 99.5\%$) with a grain size of ~ 300 nm was purchased from Alfa Aesar. Figure 1 shows the XRD pattern and an SEM image of the initial powder. It can be clearly seen that the diffraction peaks are consistent with the standard card (JCPDS No. 88-1030) of $LiMn_2O_4$. No impurities could be detected. The SEM image shows that the particles have an irregular shape and a flat surface with an average size of ~ 300 nm.

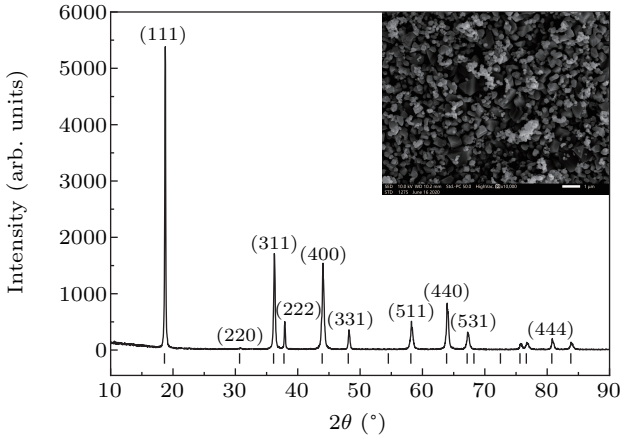


Fig. 1. XRD pattern and SEM image of the initial $LiMn_2O_4$ powder.

HTHP experiments were carried out in a cubic press (DS6 × 14 MN, China). The structure of the six-sided top press includes a power distribution system, heating system, supercharger, hydraulic station, and the main machine (base and six groups of working cylinders). The six working cylinders are divided into three fixed cylinders (lower, rear, left) and three moving cylinders (upper, front, right). The actual picture and schematic diagram of the cubic press are shown in Figs. 2(a) and 2(b). Under the push of hydraulic oil, the corresponding top hammer of the six cylinders moves to the center and extrudes the assembly. The pressure and temperature are gradually increased by the setting program, which can assure HT and HP conditions at the same time. For HTHP sintering experiments, the density of the initial material has an important effect on the shrinkage and densification behavior of the sample. The lesser the volume shrinkage and the greater the pressure transfer efficiency results in closer intergranular bonding. In other words, the higher density of the initial powder can lead to a better densification effect under the same pressure and temperature conditions. Therefore, the initial $LiMn_2O_4$ powder was pre-pressed to improve its initial density.[14] According to calculations, the sample's relative theoretical density after pre-pressurization can reach 67% of the initial sample density, followed by the HPHT treatment described below.

The standard B assembly designed in our laboratory is shown in Fig. 2(c). The steel ring was used as a conductive electrode. The closed cylindrical graphite tube was used as a heating source. The pyrophyllite was used as a pressure-transmitting medium for relative insertion of hydrostatic pressure. The pre-pressed specimen was surrounded by a tube containing NaCl pressure medium to provide the desired hydrostatic pressure environment.[15,16] The pressure range applied was 2.0 GPa–5.0 GPa, at a temperature range of 25 °C–100 °C. First, the oil pressure was set to the value corresponding to the cavity pressure. For example, when the cavity pressure needs to be at 4.0 GPa, the oil pressure is set at 30 MPa. When the actual oil pressure and the set value coincided, the press was placed into the pressure holding stage and the system began to heat. After reaching the set temperature, the holding time was 20 min, and the heating system was switched off. The pressure was released only after the temperature had dropped to room temperature (RT), and the sample could then be removed. The samples were embedded in bakelite powder using a XQ-2B metallographic sample setting machine and then polished on both sides in a Unipol-802 fine polishing machine for further testing and analysis.

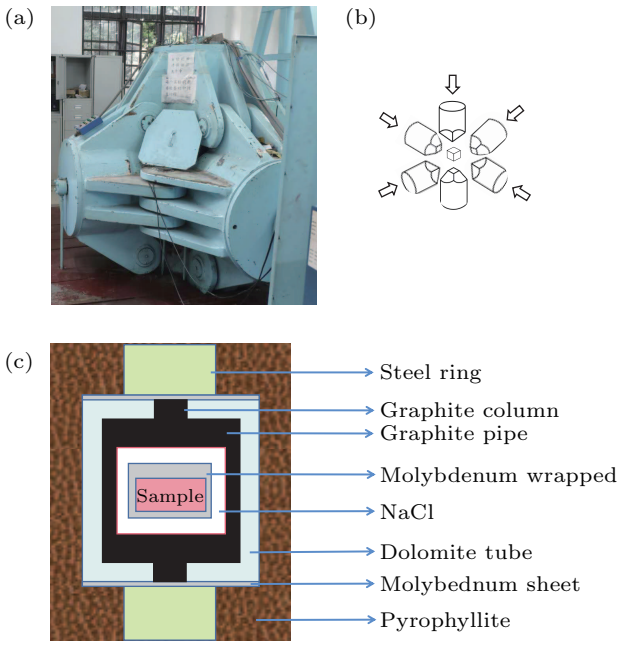


Fig. 2. (a) Actual picture of the cubic press, (b) schematic diagram of the cubic press. (c) Experimental assembly structure schematic diagram (standard B) for the HPHT experiment.

XRD phase analysis was carried out using a Dandong square circle DX2700 x-ray diffractometer. The working conditions of the diffractometer were set as 30 mA, 40 kV, Cu-$K\alpha$ radiation ($\lambda = 0.15404$ nm), the stepping mode was selected, the step size was set as 0.03 °/s, and the Bragg–Brentano mode was θ–2θ. The morphology, structure, and size of the prepared sample were observed by SEM (JSM-IT500HR, JEOL, Akishima, Japan).

3. Results and discussion

3.1. Phase identification and diffraction peak analysis

The XRD patterns from all samples obtained from the HTHP experiments at pressures of 2.0 GPa (normal pressure and temperature (NPT)-1000 °C), 3.0 GPa (NPT-700 °C), 4.0 GPa (NPT-700 °C) and 5.0 GPa (NPT-700 °C) are shown in Figs. 3(a)–3(d).

At a pressure of 2.0 GPa (Fig. 3(a)), the structure of $LiMn_2O_4$ was found stable at RT up to 600 °C. Several additional diffraction peaks started to appear at ∼ 700 °C, which were associated with orthorhombic Mn_2O_3, monoclinic Li_2MnO_3 and tetragonal Mn_3O_4. It is indicated that Mn_2O_3 appeared first. It should be noted that certain peaks in Fig. 3(a) are from the sample holder.

Similarly, figure 3(b) shows the XRD patterns of the HPHT (3.0 GPa, RT–700 °C) samples. The spinel structure was preserved up to 500 °C, and decomposition into the same three additional phases as before started at 600 °C. Some traces of Mn_2O_3, $Li_{1.05}Mn_2O_4$, and Li_2O_2 were also observed at 700 °C. At a higher pressure of 4.0 GPa, a total of four decomposition products appeared at a lower temperature of ∼ 300 °C, as shown in Fig. 3(c). These are orthorhombic Mn_2O_3, monoclinic Li_2MnO_3, tetragonal Mn_3O_4, and orthorhombic $Li_{1.13}Mn_2O_4$ with space group *Fddd*. It is worth noting that these decomposition products are not the same as before at 2.0 GPa and 3.0 GPa.

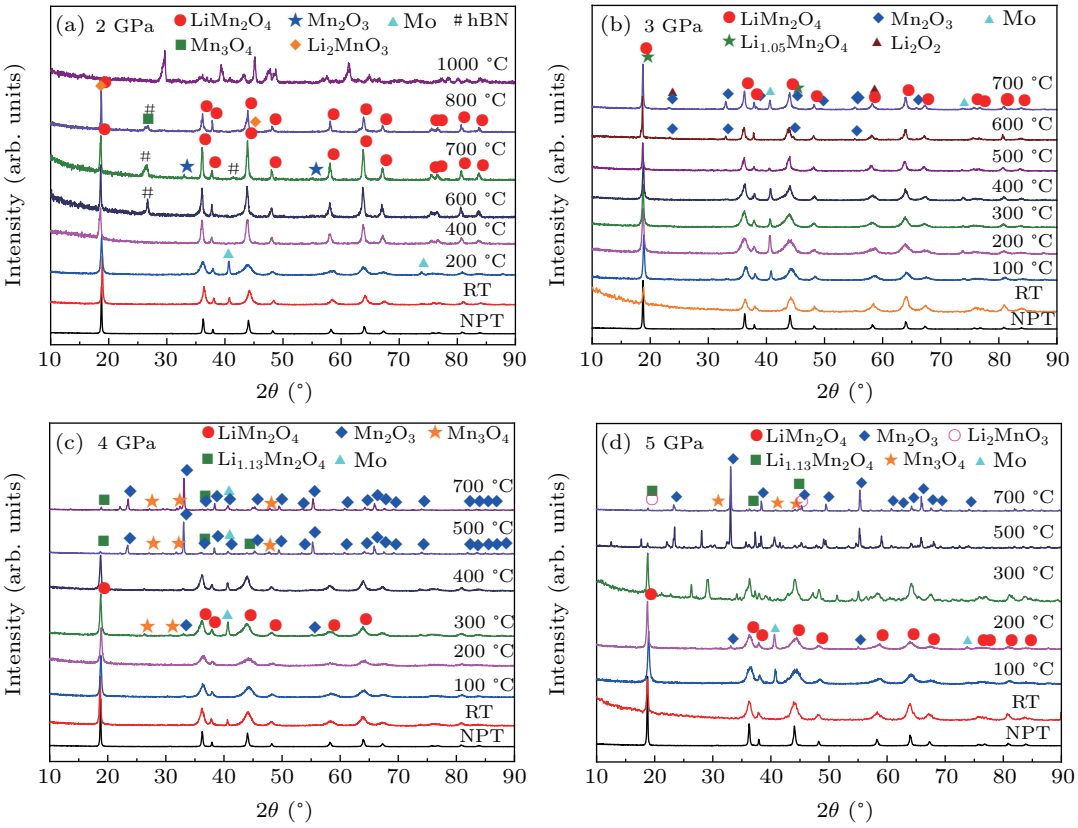


Fig. 3. XRD spectra at pressures of (a) 2.0 GPa (NPT-1000 °C), (b) 3.0 GPa (NPT-700 °C), (c) 4.0 GPa (NPT-700 °C), and (d) 5.0 GPa (NPT-700 °C).

Figure 3(d) shows the XRD patterns of the HPHT (5.0 GPa, RT–700 °C) samples. Mn_2O_3, Li_2MnO_3, $Li_{1.13}Mn_2O_4$, and Mn_3O_4 are the four phases present at 700 °C. Mn_2O_3 appeared first at 200 °C as the initial decomposition product. Below the decomposition temperature of 200 °C, including at RT, the structure of $LiMn_2O_4$ was stable at the maximum applied pressure of 5.0 GPa.

Based on the XRD patterns of all the HTHP experiment-prepared samples, it can be concluded that the decomposition temperature decreases with increasing pressure from 700 °C at 2.0 GPa, to 600 °C at 3.0 GPa, to 300 °C at 4.0 GPa and to 200 °C at 5.0 GPa. Therefore, the high-pressure treatment leads to decomposition at lower decomposition temperatures.

Figure 4 shows a series of *in-situ* powder XRD patterns collected at variable temperatures at ambient pressure. The structure of $LiMn_2O_4$ was stable at RT up to 1200 °C. When the temperature reached 1400 °C, several decomposition products appeared. These are Li_2MnO_3 with space group $C2/c$, orthorhombic $LiMnO_2$ with space group *Pmnm* and tetragonal Mn_3O_4 with space group $I41/amd$. These results indicate that the decomposition temperature of $LiMn_2O_4$ under ambient pressure is between 1200 °C–1400 °C. It should be noted that this is a higher temperature as compared to the 1000 °C reported by Thackeray *et al.*[17] However, we had carefully

calibrated our furnaces during all the *in-situ* high-temperature experiments and muffle furnace high-temperature heat treatment experiments, and we can, therefore, confirm that the experimental results presented here are reliable.

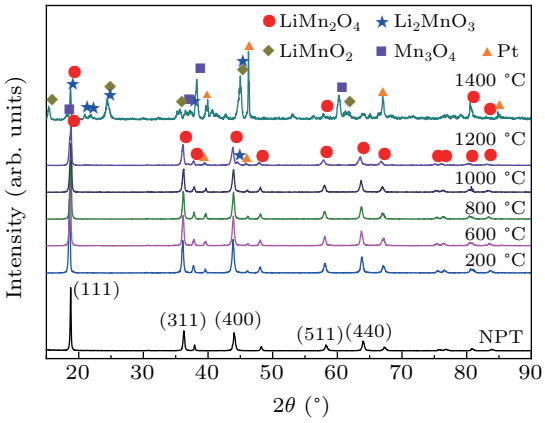


Fig. 4. *In-situ* XRD patterns of $LiMn_2O_4$ recorded at NPT to 1400 °C. If a small amount of sample is placed on the Pt substrate, some Pt diffraction peaks appear.

The variation of decomposition temperature of $LiMn_2O_4$ with pressure is shown in Fig. 5. As mentioned before, the application of high pressure leads to the decrease of decomposition temperature, i.e., the $LiMn_2O_4$ phase is less stable under high pressure, at least at high temperatures. At 5.0 GPa, the decomposition temperature is only 200 °C, which is 15% of the decomposition temperature at ambient pressure.

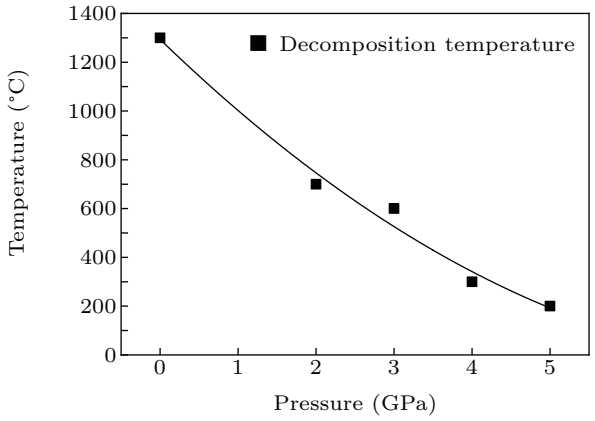


Fig. 5. The decomposition temperature of $LiMn_2O_4$ versus pressure.

Since $LiMn_2O_4$ could not decompose at room temperature under any pressure up to 5 GPa, additional experiments were conducted under 8.0 GPa (RT), but $LiMn_2O_4$ still did not decompose. In addition, by comparing the decomposition products at each pressure in Fig. 3, Mn_2O_3 was always the first decomposition product that appeared above the respective decomposition temperature, except at ambient pressure. It may, therefore, be concluded that the occurrence of Mn_2O_3 may be related to the stress-induced phase transition in the crystal structure during HP conditions.

The crystal structure of $LiMn_2O_4$ is shown in Fig. 6(a). In the unit cell of $LiMn_2O_4$, Mn^{3+}/Mn^{4+} cations occupy 16*d* octahedral positions, whereas Li^+ cations occupy the 8*a* position of the tetrahedron. From this structural diagram combined with the bond valence of $LiMn_2O_4$, it may be assumed that electrons move in the three-dimensional conduction pathways formed by Li^+ when $LiMn_2O_4$ is charged and discharged. In the HTHP experiment, O^{2-} anions changed from the original 32*e* site position to the 24*c* positions, and part of the manganese cations moved to the 8*a* and 12*b* positions. The MnO_6 octahedra are distorted due to high pressure and the Jahn–Teller instability of the Mn^{3+} (d^4) ions. Mn_2O_3 is formed under this action, as shown in Fig. 6(b). Therefore, it is plausible that MnO_6 octahedra may not distort and may not form Mn_2O_3 in the absence of pressure. This argument may be supported by the fact that at ambient pressure, $LiMn_2O_4$ decomposes at a high temperature of 1300 °C, where the decomposition products are different as compared to the samples treated at high pressure, as mentioned above.

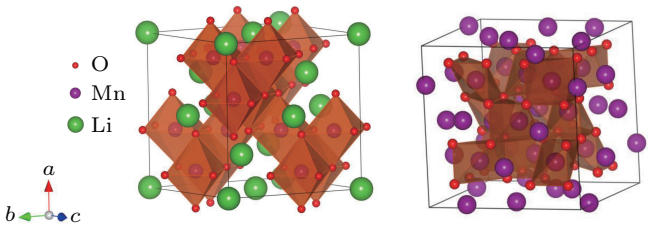


Fig. 6. Crystal structures of (a) $LiMn_2O_4$ and (b) Mn_2O_3.

To ensure the accuracy and reliability of the SEM analysis, different areas of the sample were scanned by SEM. Representative images for the initial powder at ambient pressure (1400 °C), HP (2.0 GPa, RT), HPHT (2.0 GPa, 1000 °C), HP (3.0 GPa, RT), HPHT (3.0 GPa, 600 °C), HP (4.0 GPa, RT), HPHT (4.0 GPa, 300 °C), HP (5.0 GPa, RT) and HPHT (5.0 GPa, 200 °C) were selected, as shown in Fig. 7. The primary particles of the initial powder appeared smooth and flat with an average particle size of ∼ 300 nm (Fig. 7(a)). Figure 7(b) illustrates the microstructure of the sample with an average grain size of ∼ 30 μm when heated at 1400 °C. At 1400 °C, the grain size of the sample increased significantly as compared to the starting powder, as shown in Fig. 7(a), and the grain surfaces exhibited pores resulting from gas production.

The particles became more clustered due to the HP environment at RT, as demonstrated in Figs. 7(c), (e), 7(g), and 7(i). The grains became relatively dense after the cold pressing treatment. Smaller particles appeared evenly distributed around the large particles. This may be interpreted as a result of grains breaking into smaller ones under the action of pressure. This is supported by the notion that most of the grains

are broken at the edges and corners, and the average size of the individual particles after high pressure is smaller than the initial particles. It should be further noted that the application of high pressure also leads to a particle agglomeration. However, the particle morphology and size drastically change with increasing temperature under various pressures, as shown in Figs. 7(d), 7(f), 7(h), and 7(j). In Figs. 7(d) and 7(j), the grain boundaries are blurred between the grains. The grains become denser under the action of pressure, while the grains grow with the increase in temperature. This grain growth process is clearly illustrated in Fig. 7(f), where such growth is accompanied by the precipitation of microcrystals on the surface. On the other hand, figure 7(h) also demonstrates that the grain surface has obvious growth striations.

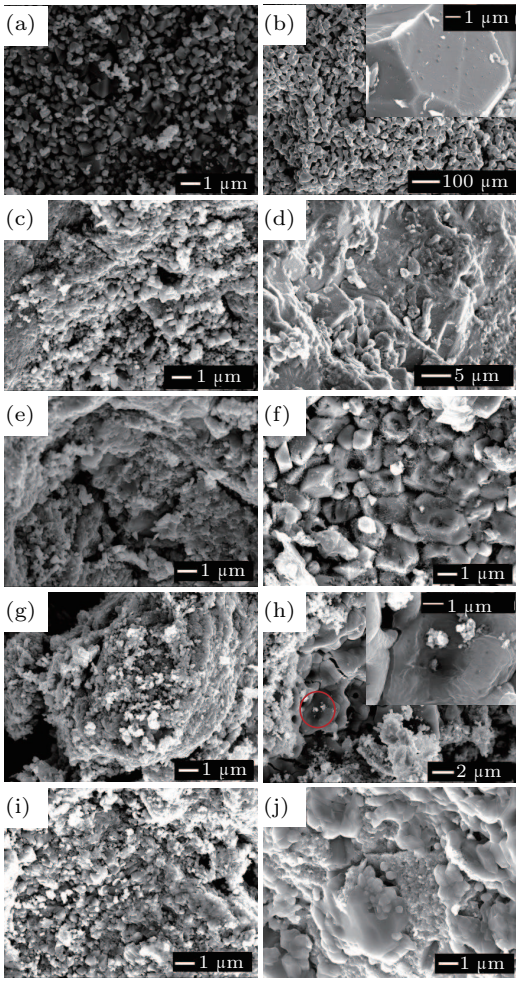


Fig. 7. SEM images of $LiMn_2O_4$ (a) initial powder, (b) at ambient pressure (1400 °C), (c) HP (2.0 GPa, RT), (d) HPHT (2.0 GPa, 1000 °C), (e) HP (3.0 GPa, RT), (f) HPHT (3.0 GPa, 600 °C), (g) HP (4.0 GPa, RT), (h) HPHT (4.0 GPa, 300 °C), (i) HP (5.0 GPa, RT), (j) HPHT (5.0 GPa, 200 °C).

From these results, it can be concluded that the grains change significantly when approaching the decomposition conditions. Meanwhile, pressure and temperature change the size and morphology of the grains, which may well be relevant for future studies on the modification and application of lithium manganate.

4. Conclusion

In summary, we performed high pressure and high-temperature experiments on the $LiMn_2O_4$ spinel phase. *In-situ* hightemperature XRD was employed to investigate the influence of pressure on the decomposition temperature of $LiMn_2O_4$. The resulting products were characterized by conventional XRD and SEM to probe the microstructure evolution, phase composition and decomposition temperature of $LiMn_2O_4$ under high temperature and high pressure. The results show that both the decomposition temperature and the decomposition products of $LiMn_2O_4$ had a strong dependence on pressure. The decomposition temperature of $LiMn_2O_4$ dropped sharply from 1300 °C to 200 °C when the pressure was increased from ambient to 5.0 GPa. This suggests that pressure may reduce the distance between atoms. On the other hand, the compound is stable at RT, even at a maximum pressure of 8.0 GPa. Therefore, it can be concluded that the decomposition of $LiMn_2O_4$ is more sensitive to temperature than to pressure. Interestingly, high pressure can promote more complex decomposition products. In the case of Mn_2O_3, this can be attributed to Jahn–Teller distortions which are enhanced under high pressure.

Acknowledgments

Project supported by the National Natural Science Foundation of China (Grant No. 12074273) and the Doctoral Research Fund of Southwest University of Science and Technology (Grant No. 20zx7136).

References

[1] Ohzuku T, Kitagawa M and Hirai T 1990 *Cheminform* **21**
[2] Tarascon J M, Wang E, Shokoohi F K, McKinnon W R and Colson S 1991 *J. Electrochem. Soc.* **138** 2859
[3] Thackeray M M 1992 *J. Electrochem. Soc.* **139** 363
[4] Thackeray M M 1995 *J. Electrochem. Soc.* **142** 2558
[5] Mukai K, Sugiyama J, Ikedo Y, Nozaki H and Chow K H 2010 *J. Phys. Chem. C* **114** 11320
[6] Ellis B L, Lee K T and Nazar L F 2010 *Chem. Mater.* **22** 691
[7] Chen Y, Xie K, Pan Y, Zheng C and Wang H 2011 *Chin. Phys. B* **20** 028201
[8] Luo N, Li X, Sun Y and Wang X 2010 *J. Alloys Compd.* **505** 352
[9] Paolone A, Sacchetti A, Postorino P, Cantelli R, Congeduti A, Rousse G and Masquelier C 2005 *Solid. State. Ion.* **176** 635
[10] Kazunari Y, Qingzhen H, Lianqi Z, Kazunori T, Yuji B, Takuro N, Yoshio M, Kosuke K and Eiji T M 2006 *J. Am. Chem. Soc.* **128** 9448
[11] Mukai K, Uyama T and Yamada I 2019 *ACS. Omega.* **4** 6459
[12] Lin Y, Yang Y, Ma H, Cui Y and Mao W L 2011 *J. Phys. Chem. C* **115** 9844
[13] Darul J, Nowicki W, Lathe C and Piszora P 2011 *Radiat. Phys. Chem.* **80** 1014
[14] Shang T, Xiao D, Zhang Q, Wang X, Su D and Lin G 2021 *Chin. Phys. B* **30** 078202
[15] Wang H, He D, Tan N, Wang W, Wang J, Dong H, Ma H, Kou Z, Peng F, Liu X and Li S 2010 *Rev. Sci. Instrum.* **81** 116102
[16] Wang H K, He D W, Yan X Z, Xu C, Guan J W, Tan N and Wang W D 2011 *High Press. Res.* **31** 581
[17] Thackeray M M, Mansuetto M F, Dees D W and Vissers D R 1996 *Mater. Res. Bull.* **31** 133